

Investigation of landslide failure mechanisms adjacent to lignite mining operations in North Bohemia (Czech Republic) through a Limit Equilibrium / Finite Element modelling approach

Claudio Vanneschi,^{a,*} Matthew Eyre,^a Jan Burda,^b Lukáš Žižka,^b Mirko Francioni,^{ac} and John S. Coggan^a

^a Camborne School of Mines, University of Exeter in Cornwall, Penryn, Cornwall, U.K.

^b Brown Coal Research Institute, Most, Budovatel, 2830, Czech Republic

^c Department of Engineering and Geology, University of Chieti-Pescara, Chieti, Italy

*Corresponding author. E-mail addresses: c.vanneschi2@exeter.ac.uk (C. Vanneschi)

Abstract

Understanding the impact of data uncertainty is a fundamental part of ensuring safe design of manmade excavations.

Although good levels of knowledge are achievable from field investigations and experience, a natural geological environment is subject to intrinsic variability that may compromise the correct prediction of the system response to the perturbations caused by mining, with direct consequences for the stability and safety of the operations.

Different types of geoscientific evidence, including geological, geomorphic, geotechnical, geomatics, and geophysical data have been used to develop and perform two-dimensional Limit Equilibrium and Finite Element Method stability analyses of a lignite open-pit mine in North Bohemia (Czech Republic) affected by recent landslides. A deterministic-probabilistic approach was adopted to investigate the effect of uncertainty of the input parameters on model response.

The key factors affecting the system response were identified by specific Limit Equilibrium sensitivity analyses and studied in further detail by Finite Element probabilistic analyses and the results were compared. The work highlights

that complementary use of both approaches can be recommended for routine checks of model response and

interpretation of the associated results. Such an approach allows a reduction of system uncertainty and provides an

improved understanding of the landslides under study. Importantly, two separate failure mechanisms have been

identified from the analyses performed and verified through comparisons with inclinometer data and field observations.

The results confirm that the water table level and material input parameters have the greatest influence on the stability of the slope.

Keywords: Numerical modelling; Limit equilibrium method; Finite element methods; Probabilistic analyses.

30 **1 Introduction**

31 Analysis of slope stability is an important part of the design of human-made excavations and understanding of potential
32 instability or evolution of natural slopes. Several different methods that analyse stability have been developed over the
33 years with added sophistication and detail, thanks to improved knowledge and technological advances, as summarized
34 by Francioni et al. (2017). Nevertheless, the uncertainty of model input data can frequently lead to simplification of
35 methods to reduce the number of variables employed to obtain useful information about failure mechanisms and
36 associated risk analyses. Traditional Limit Equilibrium Methods (LEMs) with relatively simple input(s) are, therefore,
37 still commonly used by engineers and researchers all over the world (Alejano et al., 2011; Zhou and Cheng, 2015;
38 Agam et al., 2016; Deng et al., 2016; Jiang et al., 2017; Salvini et al., 2017). LEMs, a review of which can be found in
39 Duncan (1996) and Stead et al. (2006), are simple methods where stress–strain relations are not considered and where
40 assumptions of internal force distributions are required. According to Morgenstern (1992), the latter is not a major issue
41 in practical use, because different LEMs with different assumptions provide similar results. For Factor of Safety (FoS)
42 calculations, however, instability mechanisms must be assumed a priori and this may be an important limiting factor in
43 certain contexts. To overcome such limitations, more complex numerical methods have been developed in recent years.
44 For example, in Finite Element Methods (FEMs), no assumption needs to be made regarding the failure surface (which
45 is found automatically from shear strain development), failure mechanisms, or internal force distribution (Griffiths and
46 Lane, 1999; Cheng et al., 2007). The development of FEM has allowed applications of stability analysis in complex
47 geological contexts (van den Ham et al., 2009; Francioni et al., 2015; Spreafico et al., 2016; Xie et al., 2016; Fazio et
48 al., 2017) where material deformations are accounted for, but limitations still exist that must be considered, such as long
49 run-times in the case of complex models (Francioni et al., 2014) and the increasing number of variables relative to
50 constitutive models, material parameters, and boundary and initial conditions of a given system (Cheng et al., 2007).
51 These variables all have a significant influence on the development of certain stress/strain conditions within the model.
52 Therefore, although FEMs allow for more complex and potentially more reliable analyses, the level of uncertainty of
53 the input parameters may increase drastically.

54 Another key difference between LEMs and FEMs is the FoS calculation. Generally in LEM analyses, the FoS is
55 calculated from the ratio of resisting moments to overturning moments, whereas in FEM analyses more complex
56 techniques are applied. In this paper we focus on the Strength Reduction Technique (SRT), which is applied by
57 reducing the shear strength of a material, bringing the model to a limit equilibrium state. Several applications of the
58 SRT can be found in the literature, including Zienkiewicz et al. (1975), Naylor (1982), Matsui and Sun (1992), Ugai
59 and Leshchinsky (1995), Griffiths and Lane (1999), Zheng et al. (2005), Wei et al. (2009), Tschuchnigg et al. (2015),
60 and Ma et al. (2017).

61 In addition, FEM analyses may be incapable of determining other failure surfaces, which may be only slightly less
62 critical than the SRT solution but still require investigation and potential remediation as part of good engineering
63 practice (Cheng et al., 2007). When using the FEM/SRT method, it is common to have strain localization with the
64 formation of a unique failure surface. Other possible simultaneous failure mechanisms, however, may not be easily
65 identified. This is one of the reasons why Cheng et al. (2007) suggested that LEM and FEM analyses should be
66 performed together as a routine check.

67 Stead et al. (2006) provided a review of developments of numerical modelling techniques and applications for
68 characterization of complex rock slopes, illustrating how deformation and failure analyses may be undertaken using
69 three levels of sophistication. These levels include conventional LEMs (level I), FEMs (level II), and hybrid methods
70 (level III). In this paper, we have adopted a complementary approach that combines the use of the first two levels of
71 analysis to optimize the workflow and reduce the degree of uncertainty. In open-pit mining operations, understanding
72 the potential impact of data uncertainty within a geotechnical model is necessary to ensure efficient design of a mine.
73 Data uncertainties derive from the recurrent difficulties in correctly predicting the inherently variable properties and
74 characteristics of natural materials, which can be characterized into three groups: geological uncertainty, parameter
75 uncertainty, and model uncertainty.

76 According to Read (2009), these can be summarized as follows:

77 *Geological uncertainty* refers to the unpredictability associated with the identification and geometry of the different
78 lithologies and structures which constitute the geological model and the mutual relationships between them. It
79 encompasses, for example, uncertainties arising from features such as incorrectly delineated lithological boundaries and
80 major faults as well as unforeseen geological conditions.

81 *Parameter uncertainty* embraces the unpredictability of the parameters used to account for the various attributes of the
82 geotechnical model. Typically, this includes uncertainties associated with the values adopted for rock mass and
83 hydrogeological model parameters, such as the friction angle, cohesion, deformation moduli, and pore pressures.

84 *Model uncertainty* accounts for the unpredictability that surrounds the selection process and the different types of
85 analyses used to formulate the slope design and estimate the reliability of the pit walls. Examples include the various
86 two-dimensional LEMs/FEMs stability analysis methods and the more recently developed three-dimensional numerical
87 stress and displacement analyses now used in pit slope design. Model uncertainty exists if the possibility of obtaining an
88 incorrect result exists even if exact values are available for all the model parameters.

89 Based on the authors' experience, given the uncertainty present in natural contexts, a minimum FoS of 1.3 is suggested
90 for reasonable assurance of safe slope design. The use of $FoS < 1.3$ and $FoS < 1.5$ as criteria is a useful addition to FoS
91 < 1.0 in analyses where $FoS = 1.0$ is necessarily a small value that does not assure safe design. In this regard,

92 acceptance criteria and interpretations suggested by Priest and Brown (1983), with proposed modifications by Pine
93 (1992), consider a minimum FoS of 1.5 for interpretation of slope stability analyses.

94 Using a case study from an open-pit mine located in North Bohemia (Czech Republic), this paper demonstrates the use
95 of different geoscientific evidence collected over recent years (geological, geomorphic, geotechnical, geomatics, and
96 geophysical data) to back-analyse the reactivation of the landslide through an approach that involves two-dimensional
97 LEM and FEM stability analyses.

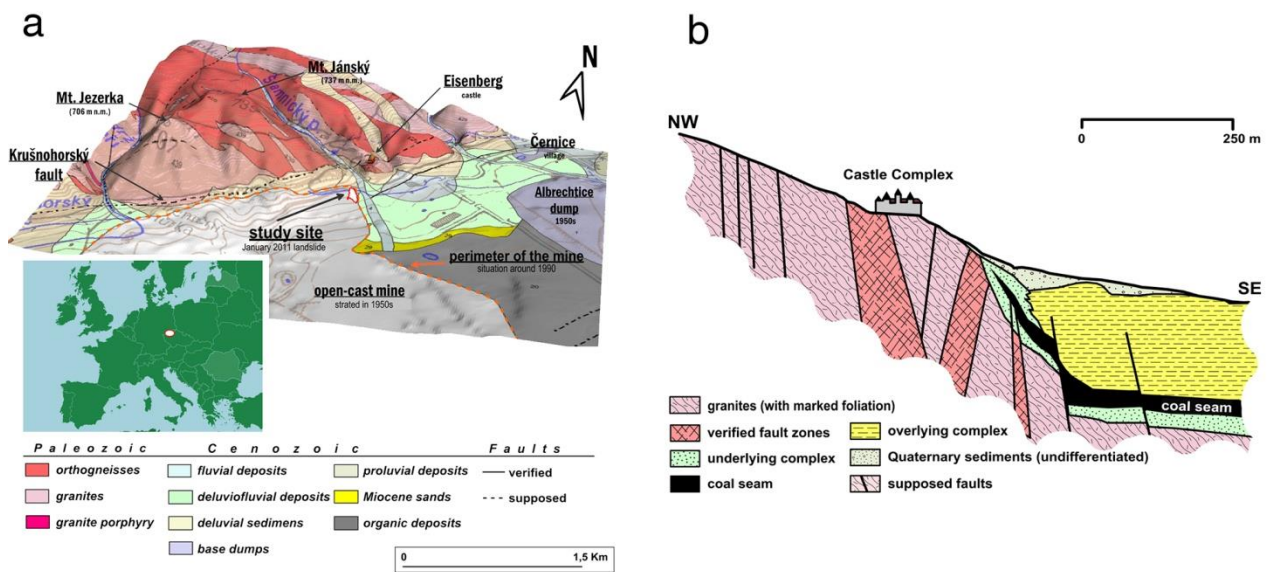
98 Uncertainty is considered through performing initial sensitivity analyses, which are simple and time efficient because
99 only a single variable is altered at a time, as well as more complex probabilistic analysis. Finally, the developed models
100 are compared with field information, from direct observations to geotechnical inclinometer data interpretation, to
101 calibrate and validate the models, making sure that the results are consistent with real observations. The potential for the
102 presence of two separate failure mechanisms, one associated with deep-seated instability and the other linked to shallow
103 superficial slope deformation, is also investigated.

104 For this case study, the Rocscience Slide7.0 and RS² software applications (Rocscience, 2017a) were used respectively
105 for LEM and FEM analyses. The two-dimensional approach was chosen to decrease the level of model/geological
106 uncertainty given that the case study area has a complex geometry and therefore a representative three-dimensional
107 reconstruction is still difficult to achieve. For this reason, the authors preferred to simplify the analyses to improve the
108 understanding of the dominant mechanism that affects the response of the system. In the authors' experience,
109 complexity should be carefully studied before being included in numerical models, especially if increasing the number
110 of variables reduces the level of control of the model response. Three-dimensional analyses may be performed,
111 however, in further research following improved understanding of failure mechanisms from the two-dimensional
112 simulations. Such back-analyses can help to improve the understanding of landslide processes, evaluate the effects of
113 data uncertainty, and provide guidelines for mine or slope design purposes.

114 **2 Geological setting**

115 The study area is located in North Bohemia, where the Československá Armáda (ČSA) open-pit mine is located at the
116 edge of the Mostecká Pánev Basin and the crystalline massif of the Krušné Hory Mountains (Fig. 1a).

117 With a depth of approximately 200 m, ČSA open-pit mine was the deepest mine in Czech Republic until 2009 and is
118 formed by a high anthropogenic slope that passes smoothly (with an inclination of 10–15°) into the steep slopes of the
119 Krušné Hory Mountains behind the margin of the basin (Burda et al. 2011). A schematic geological cross-section of the
120 area is provided in Fig. 1b.



121

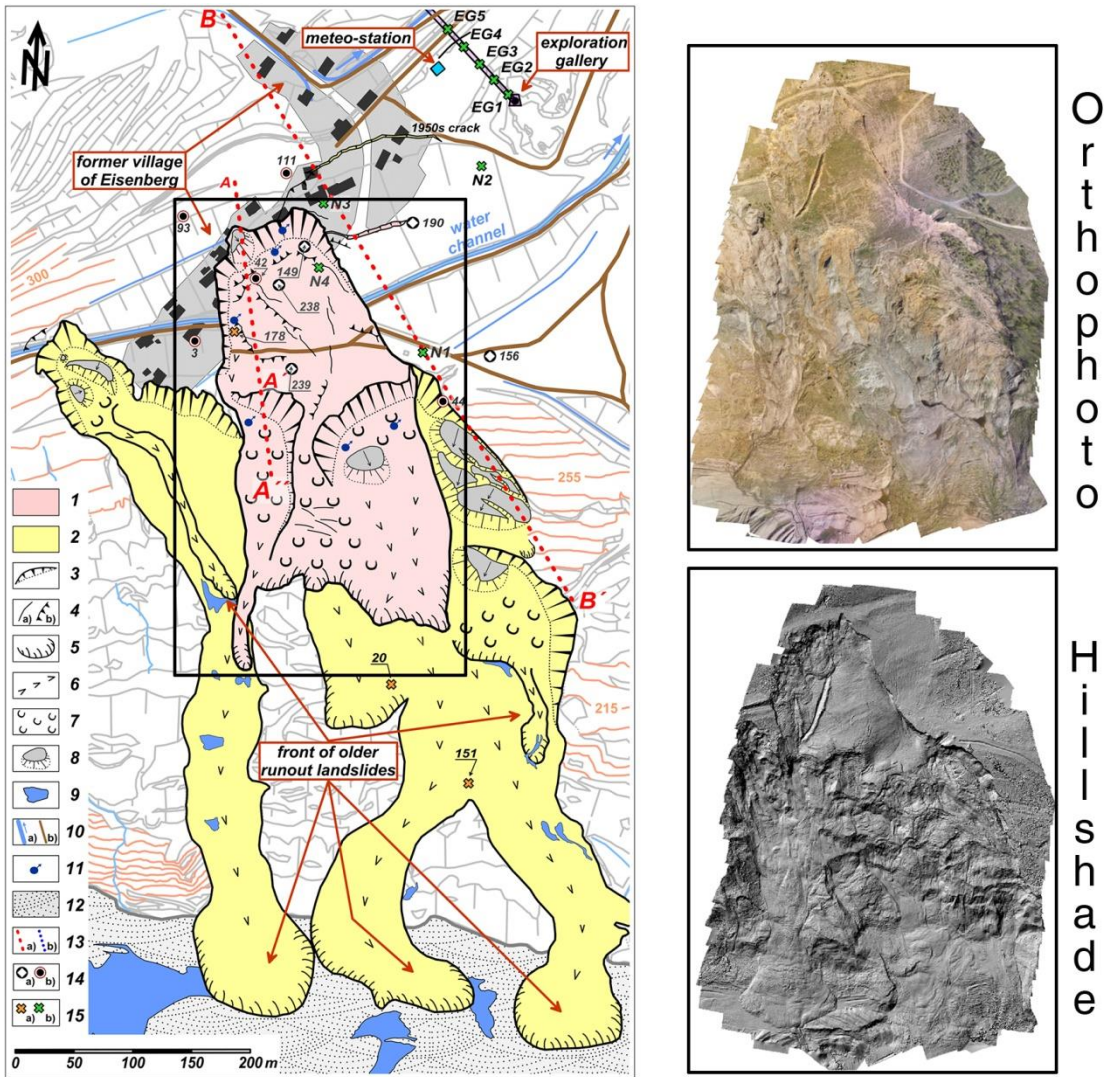
122 **Fig. 1.** General topographic and geological overview with inset map showing the study area location (a) and geological cross-section
 123 through the edge of the Most Basin and Krušné Hory Mountains (b); modified from Burda et al. (2011, 2013)
 124

125 The sedimentary basin consists of an Underlying Complex (mostly lower Miocene sandy-clays), the coal seam, and an
 126 overlying complex (composed of upper Miocene claystones and Quaternary sediments). Burda et al. (2011) reported
 127 that the underlying complex is stratigraphically heterogeneous, with Tertiary clays, sandstones, and sands as well as
 128 Cretaceous quartzite, calcareous clays, marlites, and limestones. In addition, volcanic rocks, such as basalts, phonolites,
 129 and tuffs, have also been found in this complex. The overlying complex is also made up of clays and sandy-clays with
 130 variable occurrence of carbonates (Malkovský, 1985). The Quaternary sediments are comprised of coarse-grained
 131 gravel, sandy gravel, and clays with crystalline fragments, with thicknesses ranging from 0.1 to 40 m (Burda et al.,
 132 2011).

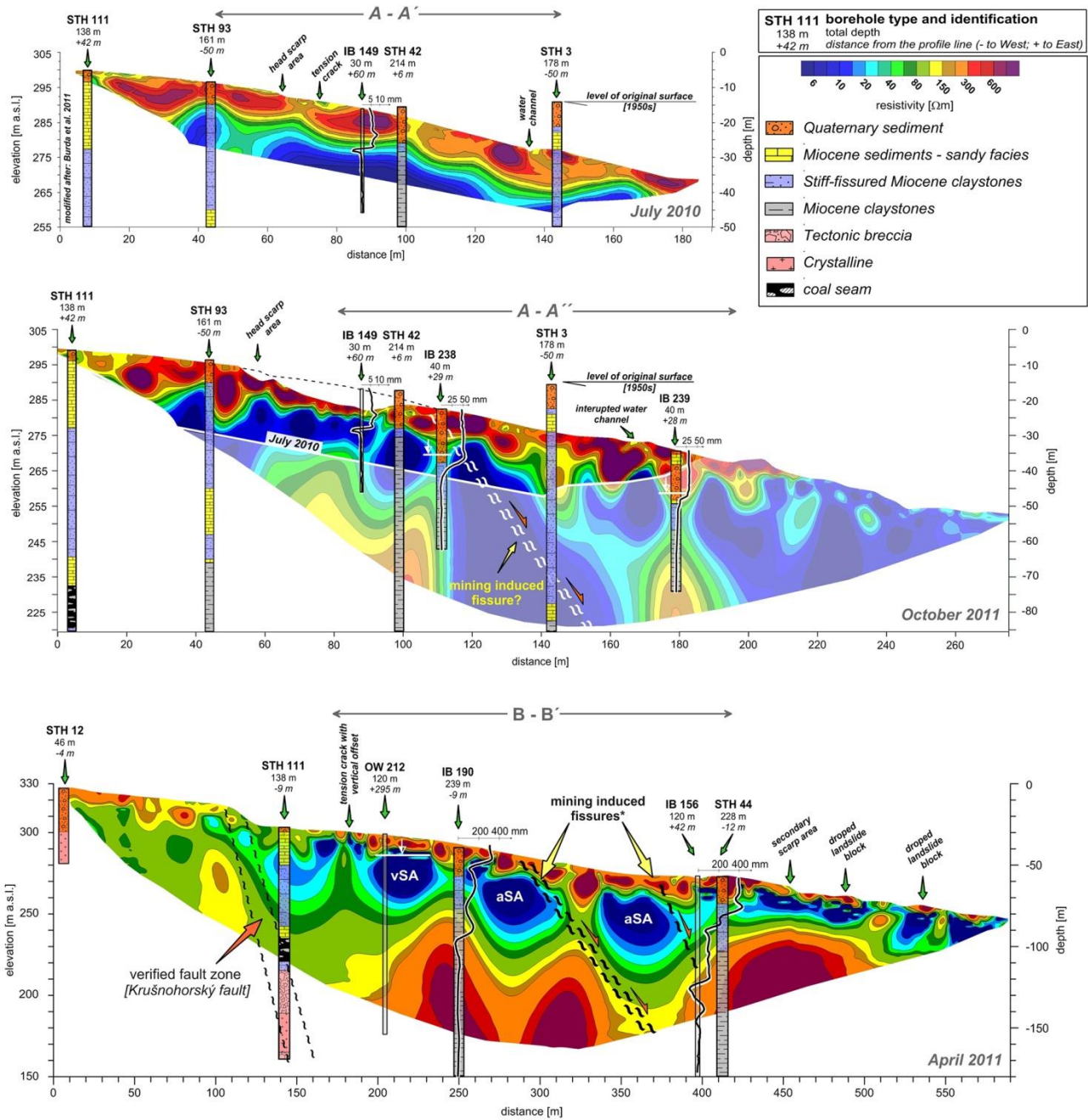
133 A dramatic slope deformation which started in 1952 (Rybář, 1997) resulted in the abandonment of the village of
 134 Eisenberg, but mining operations continued in the form of open-cast exploitation (Burda et al., 2013). According to
 135 Hurník (1982), the removal of millions of tons of overburden material per year (in the 1970s and 1980s) could have
 136 caused the elastic lifting of the mountain massif and the destabilization of the upper part of the slope. In this regard,
 137 recent studies (Burda et al., 2011; Burda et al., 2013) confirmed an influence of mining, mainly in the mountains'
 138 piedmont, where the basin sediments were exposed during excavations.

139 In January 2011, the area experienced a reactivation of the landslide, which can be related to failure of the overlying
 140 Quaternary sediments. This recent failure represented one of the largest flow-like landslides of the Czech Republic
 141 (Klimeš et al., 2009; Pánek et al., 2011) and occurred outside the active portion of the ČSA mine, with the landslide
 142 material reaching the bottom of the open-pit coal mine (Burda et al., 2013). According to Burda et al. (2013), such
 143 reactivation was triggered by a rising water table induced by rapid snowmelt during a period of winter warming. They

144 concluded that the movement accelerations occurred when a theoretical pore pressure of 68 kPa was present at the depth
 145 of the shear plane, which was approximately located at the interface between the Quaternary sediments and the Miocene
 146 claystones. As far as the drainage is concerned, a system of drainage wells was used in the 1980s and replaced with
 147 surface ditches in the 1990s after the mining activities were stopped in this part of the mine.
 148 A detailed map of the mine area affected by the landsliding is shown in Fig. 2, while Fig. 3 shows the 2D Electrical
 149 Resistivity Tomography (ERT) profiles (including boreholes, inclinometers, and piezometer data).



150
 151 **Fig. 2.** A geomorphological sketch map of the area around the landslide that occurred during January 2011: (1) the landslide of
 152 January 2011; (2) older landslides within the landslide complex; (3) headscarps; (4) (a) tension cracks, (b) tension cracks with
 153 vertical offset; (5) accumulation toes; (6) earthflows; (7) landslide accumulation surfaces; (8) landslide blocks within the landslide
 154 complex; (9) shallow colluvial depression; (10) (a) brooks and channels, (b) road; (11) spring; (12) dump; (13) (a) ERT profile, (b)
 155 longitudinal profile across the landslide; (14) (a) inclinometer borehole (b) structural test hole; (15) observed geodetic points (a) ATR
 156 – reflective prism, (b) precise levelling – bench marks (modified from Burda et al., 2013)



157
158
159
160

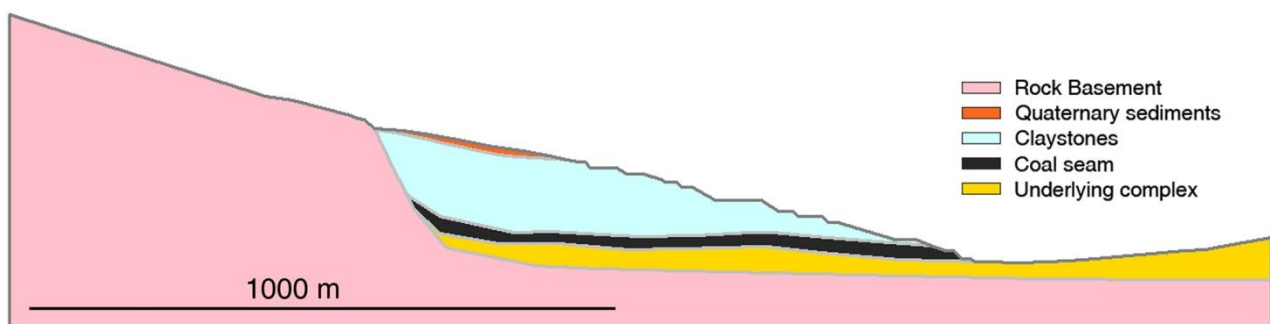
Fig. 3. The ERT profiles taken across the landslide (locations depicted in Fig. 4). STH: structural test hole; IB: inclinometer borehole; OW: observation well; vSA: verified shallow aquifer; aSA: assumed shallow aquifer (from Burda et al., 2013)

161
162
163
164
165
166

As observed from the inclinometers shown in Fig. 3, the failure surface of the reactivated landslide (profile A-A'') can be approximately located at the interface between the Quaternary sediments and the Miocene claystone (at a depth of about 10–15 m). In addition, evidence of the old deeper landslide (dated back to 1952), described as a deep-seated rotational failure (Burda et al., 2013), is present on inclinometers located along profile B-B', which is relatively close to the position of the reactivated shallow landslide. This suggests that the presence of two different failure mechanisms within the study area cannot be excluded.

167 3 Limit Equilibrium Method analyses

168 In this study, the focus was on the development of an improved understanding of the landslide reactivated in January
169 2011, which occurred along profile A-A" depicted in Fig. 2. The 2D model used in the analyses is shown in Fig. 4; it
170 considers the pre-failure shape and has been derived from the geometrical/geological information obtained from Figs. 2
171 and 3 and the topographic data provided directly by the mine. The profile of the slope has been extended to consider the
172 potential influence of extraction of the lignite at the base of the slope, which in this area is more than 200 m deep. The
173 preliminary LEM analysis regarding the effect of uncertainty was carried out by using the Slide7.0 software and
174 adopting the Mohr-Coulomb linear criterion (with parameters ϕ and c) and the vertical slice Janbu corrected method
175 (Janbu, 1973). Considering the presence of different geological strata that may influence the shape of the failure
176 surface, a non-circular surface type approach, with the Cuckoo Search method, was adopted. The Cuckoo Search
177 method (Yang and Deb, 2009) is considered a fast and efficient global method of locating non-circular critical surfaces
178 that is not affected by local minimum solutions, which may be possible when using other surface search methods (e.g.
179 block and path search).



180
181 **Fig. 4.** Longitudinal profile used for the stability analysis (no vertical exaggeration is applied)

182 3.1 Deterministic and sensitivity LEM analyses

183 For this case study, given the detailed geometrical information such as borehole data and ERT profiles, the major source
184 of uncertainty is associated with data input relating to the material properties (parameter uncertainty).

185 The first step of the sensitivity analysis was to vary the parameters across a range of values, observing the effect on the
186 final calculated FoS. Using this methodology, it is possible to determine which parameters have the most influence on
187 the stability of the slope. For a sensitivity analysis in Slide7.0 it is necessary to determine relative (distance from the
188 mean value) minimum and relative maximum values across which the analysis can be performed. This can also be
189 expressed in terms of two or three standard deviations away from the mean value. The values used (Pichler, 1989) in the
190 sensitivity analysis, based on the mine operator's laboratory test data (taken from boreholes within the ČSA mine,
191 where the majority of the geotechnical investigation focused on the basin–mountain contact area) and model calibration,
192 are shown in Table 1 (the reported parameters are intended as peak effective values). As observed, the properties

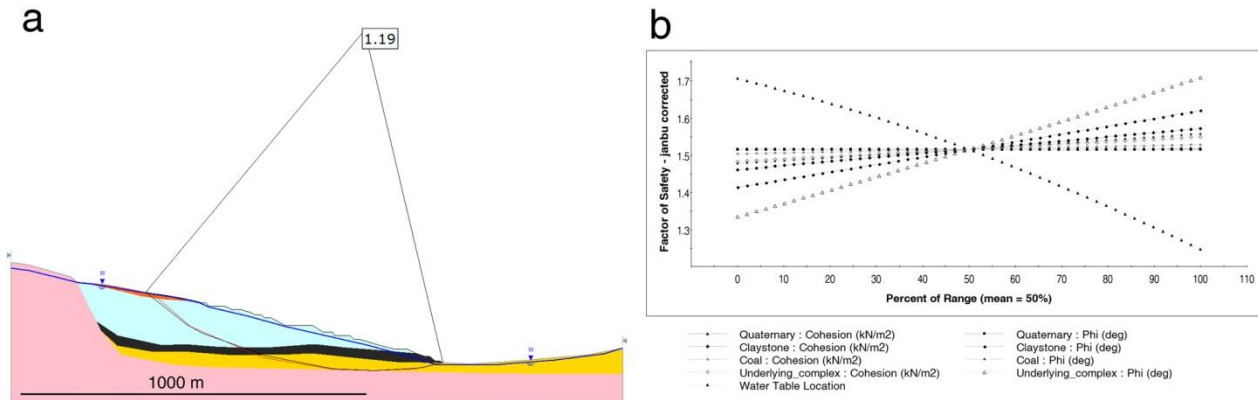
193 indicate relatively poor to weak geotechnical materials that explain the rotational movement indicated in previous
 194 analyses, which would tend to exclude pure discontinuity-controlled failure mechanisms.

195 **Table 1**
 196 Sensitivity analysis: Relative MINIMUM and MAXIMUM values for each geological formation

Material	Property	Mean	Rel. Min.	Rel. Max
Rock basement	Cohesion (kPa)	1000	500	500
Rock basement	Unit weight (kN/m ³)	25	5	5
Rock basement	Phi (°)	42	5	5
Quaternary sediments	Cohesion (kPa)	5	5	5
Quaternary sediments	Unit weight (kN/m ³)	20	5	5
Quaternary sediments	Phi (°)	27	5	5
Claystones	Cohesion (kPa)	100	50	50
Claystones	Unit weight (kN/m ³)	20	5	5
Claystones	Phi (°)	18	5	5
Coal	Cohesion (kPa)	50	25	25
Coal	Unit weight (kN/m ³)	14	5	5
Coal	Phi (°)	25	5	5
Underlying complex	Cohesion (kPa)	40	20	20
Underlying complex	Unit weight (kN/m ³)	20	5	5
Underlying complex	Phi (°)	24	5	5

197

198 The water table was also initially considered in the deterministic analysis, whose results (mean values) and associated
 199 sensitivity analysis are provided in Fig. 5.



200
 201
 202
 203

Fig. 5. Slide7.0 LEM deterministic stability analysis results with indication of global minimum FoS (a) and LEM sensitivity analysis results (b) (no vertical exaggeration is applied)

204 As observed in Fig. 5, the failure surface with the minimum FoS is a deep-seated surface that passes through the
 205 underlying complex, coal seam, and claystone layers. The analysis undertaken has not provided a good representation of
 206 the shallow failure surface that developed at the interface between the Quaternary sediments and the claystone layer. In
 207 addition, it can be seen that the modelled water location has the greatest influence on the FoS results. In particular, if the
 208 effect of water in the slope is removed, the FoS rises to about 1.7.

209 According to Burda et al. (2013), the permeability of the claystone layer is highly variable and is influenced by
 210 continuity and thickness, mainly in the upper part of the geological formation, and by the varying properties of the clay.
 211 The inclusion of a water table in the simulation, however, leads to a low FoS (< 1.3), which, given the uncertainty of

212 some input data, may indicate potential deep instability at an overall slope scale. In this context, the uncertainty related
213 to the water distribution in the slope is a major issue. The results of Pletichová (2006) and 2D ERT interpretations
214 highlighted by Burda et al. (2013) concur in identifying the presence of a high-resistivity layer formed by permeable
215 slope deposits (Quaternary sediments) that overlie a water-saturated zone, probably corresponding to the altered
216 claystone. At the base of this zone, another high resistivity area exists that most likely relates to impermeable ($< 10^{-8}$ m
217 s^{-1}) dry compact claystones. Therefore, the altered permeable claystone level is likely to hold water, resulting in perched
218 or raised water pressures and thereby creating an ideal sliding plane for the landslide. Consequently, it is possible to
219 hypothesize that deep water infiltration may also be precluded (at least in part) by the impermeable claystone level.
220 Other parameters that showed the highest influence on the FoS are the friction angle of the underlying complex and the
221 friction angle and cohesion of the claystone. This highlights the importance of good site investigation to establish,
222 where possible, the range of variation of material strength parameters.

223 **3.2 Probabilistic LEM analysis**

224 In general, the sensitivity analyses indicated that the most critical situation in this model is relative to a deep-seated
225 failure surface that involves the underlying complex, coal seam, and claystone levels and shows little to no evidence of
226 a shallow landslide involving the Quaternary sediments. Consequently, probabilistic stability analyses were carried out
227 in two stages: with initial focus on an overall slope scale and subsequent evaluation of the shallow near-surface
228 Quaternary strata.

229 In a probabilistic analysis, it is possible to associate a statistical distribution to the model input parameters, accounting
230 for the degree of uncertainty in the parameter values. In Slide7.0, input data samples are randomly generated based on
231 the user-defined statistical distribution. This results in a distribution of the FoS from which the probability of failure for
232 the slope can be calculated. The default random sampling in Slide7.0 is the Latin Hypercube Sampling method (used for
233 this analysis). With reference to the Slide7.0 user manual (Rocscience 2017b), the Latin Hypercube method is based on
234 "stratified" sampling, with random selection within each stratum. Typically, an analysis using 1000 samples obtained by
235 the Latin hypercube technique will produce comparable results to an analysis of 5000 samples using the Monte Carlo
236 method.

237 In this case, the probabilistic analysis is focused on the claystone and underlying complex parameters (highlighted by
238 previous sensitivity analysis results), including (Fig. 6a) and excluding (Fig. 6b) the water content in the deeper levels
239 (claystones, coal seam, and underlying complex, according to previous interpretations from Pletichová, 2006, and Burda
240 et al., 2013).

241 The material statistics are provided in Table 2.

242 **Table 2**
 243 Statistical properties used in the probabilistic analysis for each geological formation

Material	Property	Distribution	Mean	Std. Dev.	Rel. Min.	Rel. Max.
Claystones	Phi (°)	Normal	18	1.66	5	5
Claystones	Cohesion (kPa)	Normal	100	16.6	50	50
Underlying complex	Phi (°)	Normal	24	1.66	5	5
Underlying complex	Cohesion (kPa)	Normal	40	6.6	20	20

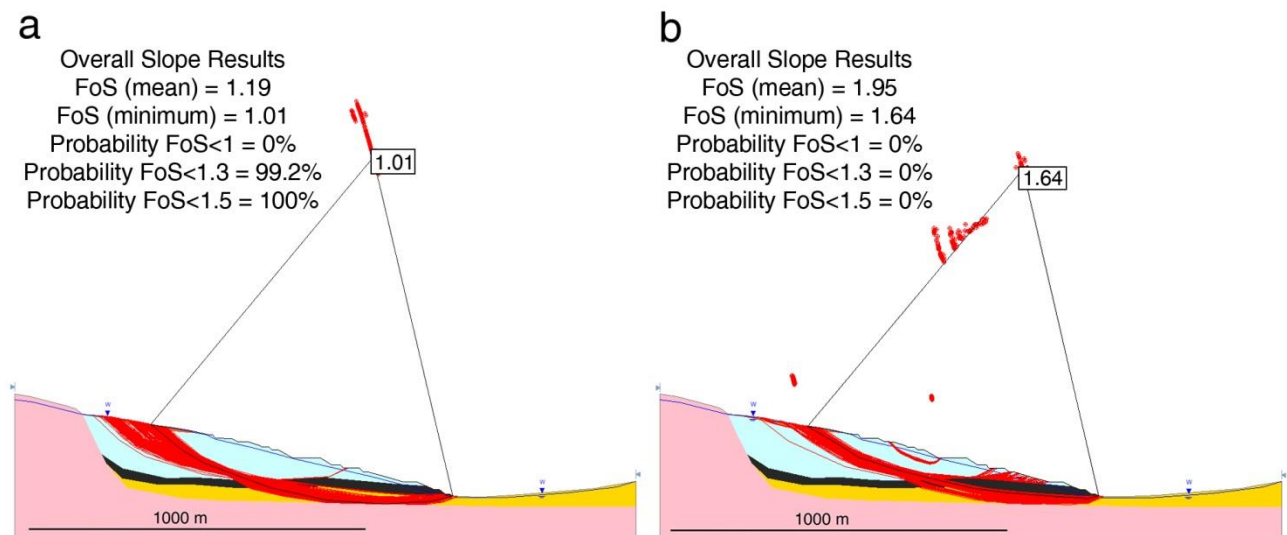
244

245 Without evidence for any other distribution, a normal distribution was adopted in this case study, with Standard
 246 Deviation (Std Dev) values estimated using the following equation (1):

247
$$\sigma = \frac{HCV - LCV}{6} \quad (1)$$

248 where HCV is the highest conceivable value of the random variable and LCV is the lowest conceivable value of the
 249 random variable (Duncan, 2000).

250 Results of the probabilistic analyses are given in Fig. 6.



251

252 **Fig. 6.** Results of Slide7.0 LEM probabilistic analyses performed including (a) and excluding (b) the effect of the water table at
 253 deeper levels (claystone, coal, underlying complex) (no vertical exaggeration is applied)

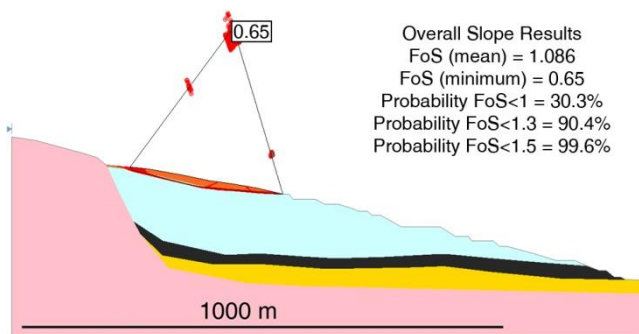
254

255 Again, the critical failure surfaces, depicted in Fig. 6, do not refer to the Quaternary strata but possible deep-seated
 256 instability on an overall scale is highlighted. The results indicate, however, a 99% probability of FoS < 1.3 in “wet”
 257 conditions and a 0% probability of FoS < 1.3 in “dry” conditions.

258 3.3 Focus on the instability of Quaternary deposits

259 The results illustrated so far show how the lowest FoS values refer to possible instability at an overall slope scale and do
 260 not replicate the superficial landslide observed at the mine site associated with the Quaternary sediments. In detail, the
 261 failure surfaces that involvet the Quaternary deposits show a minimum FoS of 2.13, with a 0% probability of failure,
 262 even considering a minimum FoS of 1.5.

263 Analysis of the data (not shown) indicates that even with a combination of low friction angle and high water table, FoS
 264 values lower than 2 are not obtained within the Quaternary sediments. This result does not match field observations,
 265 where instability on superficial strata has been detected, and a more in-depth study of the parameters of the Quaternary
 266 layer is required. For clarity, a possible hypothesis, based on what is stated in Burda et al. (2013) concerning the
 267 presence of an altered permeable claystone level at the bottom of the Quaternary sediments (mainly detected through
 268 2D ERT surveys and analysis of landslide deposit material), needs to be explained before undertaking further
 269 simulations. It is possible that in the case of abundant water infiltration, because of precipitations and snow melting
 270 during spring time, this altered claystone level may become saturated and water flow parallel to the slope may occur at
 271 the interface with an impermeable level in the claystone. Considering the low depth of this level (10–15 m) with respect
 272 to the length of the slope (more than 200 m), it is possible that under these circumstances the slope approaches a
 273 condition similar to an *infinite saturated slope*. For a saturated slope in this condition, the critical slope angle is about
 274 half that of a completely dry slope ($\tan\alpha_{crit} \sim 1/2 \tan\phi$).
 275 To try to simulate this effect, a new layer with a low friction angle (about half of that of the claystone, 9°) at the base of
 276 the Quaternary sediments was included in the model. This is aimed at simulation of the superficial alteration of the
 277 claystone layer, which could respond as a saturated soil. Results of the analysis are shown in Fig. 7. Although the
 278 natural variability of the altered layer is unknown, this analysis provides an initial starting point to assess its potential
 279 impact on the shallow landslide.



280
 281 **Fig. 7.** Result of Slide7.0 LEM probabilistic analysis focused on Quaternary sediments (no vertical exaggeration is applied)
 282

283 It is possible to see that the FoS in this case is closer to what is expected from field observations, with up to 99.6%
 284 probability of failure considering a minimum FoS of 1.5. Complex slope movements, with different deformation
 285 mechanisms, cannot be fully replicated and simulated with LEM analysis. This is because plastic deformation and
 286 degradation of material properties are not considered in such an analysis. Deformations of the deeper geological strata
 287 could have played a role in triggering the rapid and shallow landslide reactivated in January 2011. Therefore, more
 288 complex numerical modelling analyses should be carried out to fully understand the implications of the observed
 289 landslide at the mine site. An example of such analysis is described in the next section.

290 **4 Finite Elements Method analyses**

291 The analysis was carried out using the 2D FEM analysis software RS², following the same logic as the previous
 292 Slide7.0 analyses. Using the available material properties, a Mohr Coulomb failure criterion was adopted for the
 293 analyses. To simulate the plastic response of the different materials, the values highlighted in Table 3 have been
 294 adopted (approximate test data, subjected to calibration):

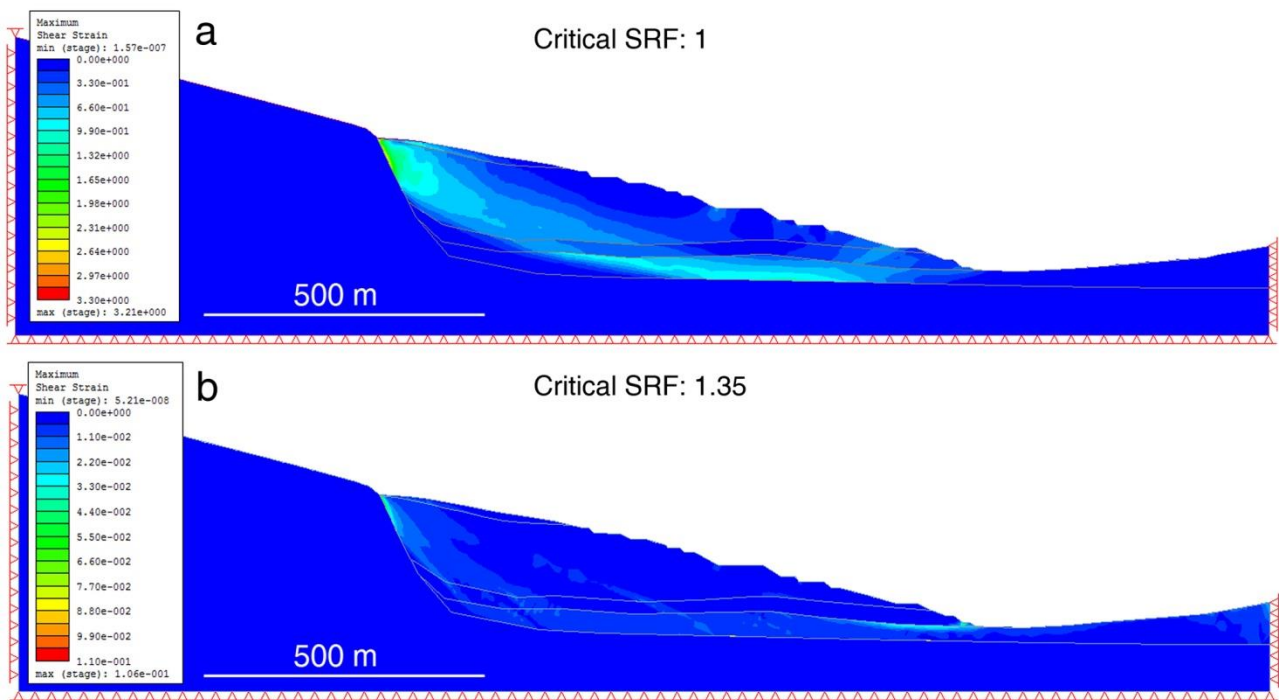
295 **Table 3**
 296 Young's modulus and Poisson's ratio utilized in the RS² FEM analysis

Material	Young's Modulus (MPa)	Poisson's Ratio
Rock basement	100000	0.2
Quaternary sediment	200	0.3
Claystone	5000	0.25
Coal seam	1000	0.3
Underlying complex	200	0.3

297
 298 To simulate the progressive mining activity undertaken at the case study site, 18 excavation stages have been included
 299 in the numerical analysis.

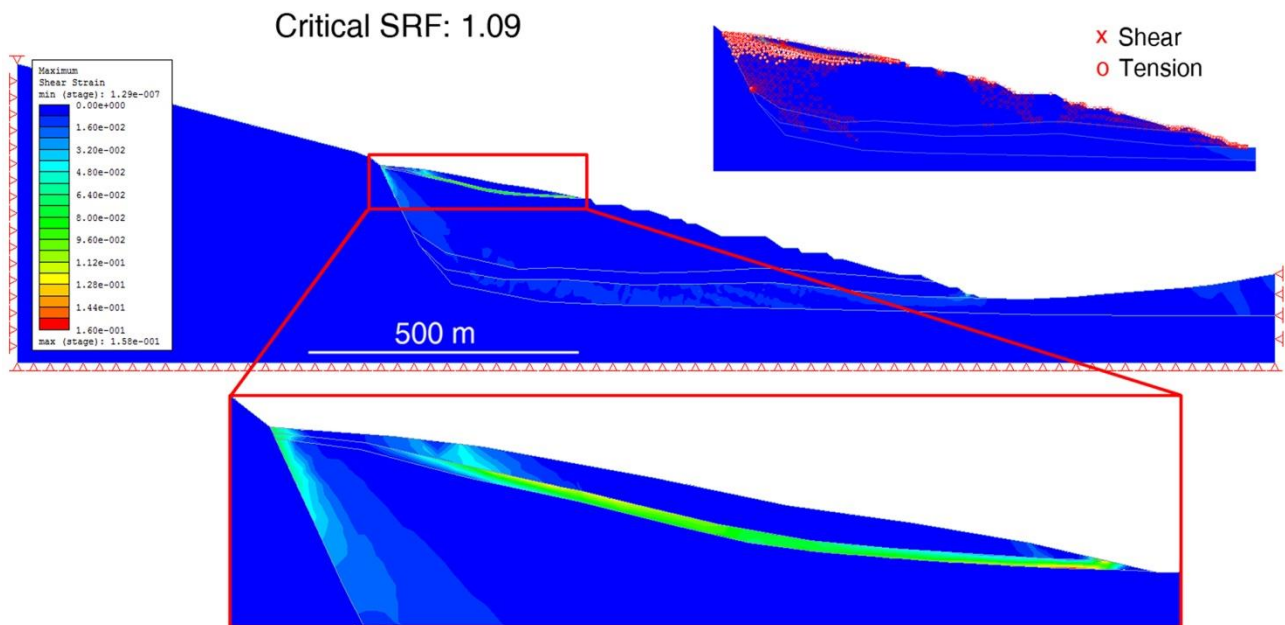
300 **4.1 Deterministic FEM analysis**

301 In keeping with previous results, the first FEM deterministic analyses have been carried out using the same profile as
 302 shown in Fig. 4, initially considering the presence of water in all geological strata (Figure 8a) and then confining it only
 303 to the Quaternary sediments (Figure 8b). The results of these analyses, which allow consideration of the effect of water
 304 level on the model, are shown in Fig. 8.



305
 306 **Fig. 8.** Shear strain development depicted in preliminary RS² numerical modelling (no vertical exaggeration is applied)
 307

308 In this case, the analyses show the development of shear strain values in deeper strata, similar to that observed from the
 309 LEM analysis. The critical detected values of the Shear Reduction Factor (SRF, calculated with the SRT; in this work
 310 SRF and FoS are used as synonyms for convenience) are equal to 1 and 1.35. The inclusion of water content in deep
 311 levels leads to very low values of the critical SRF (1) and high values of shear strain that do not match field
 312 observations. Moreover, no indication of the shallow landslide highlighted earlier in the Quaternary sediments exists.
 313 Therefore, in a similar way to what was performed with LEM analyses, a new model RS² was created including the
 314 altered claystone level. The slope was considered dry, with a low friction angle (9°) assigned to the altered claystone to
 315 simulate the effect of the water flow on the strength properties of the material. The result of the analysis is shown in
 316 Fig. 9.

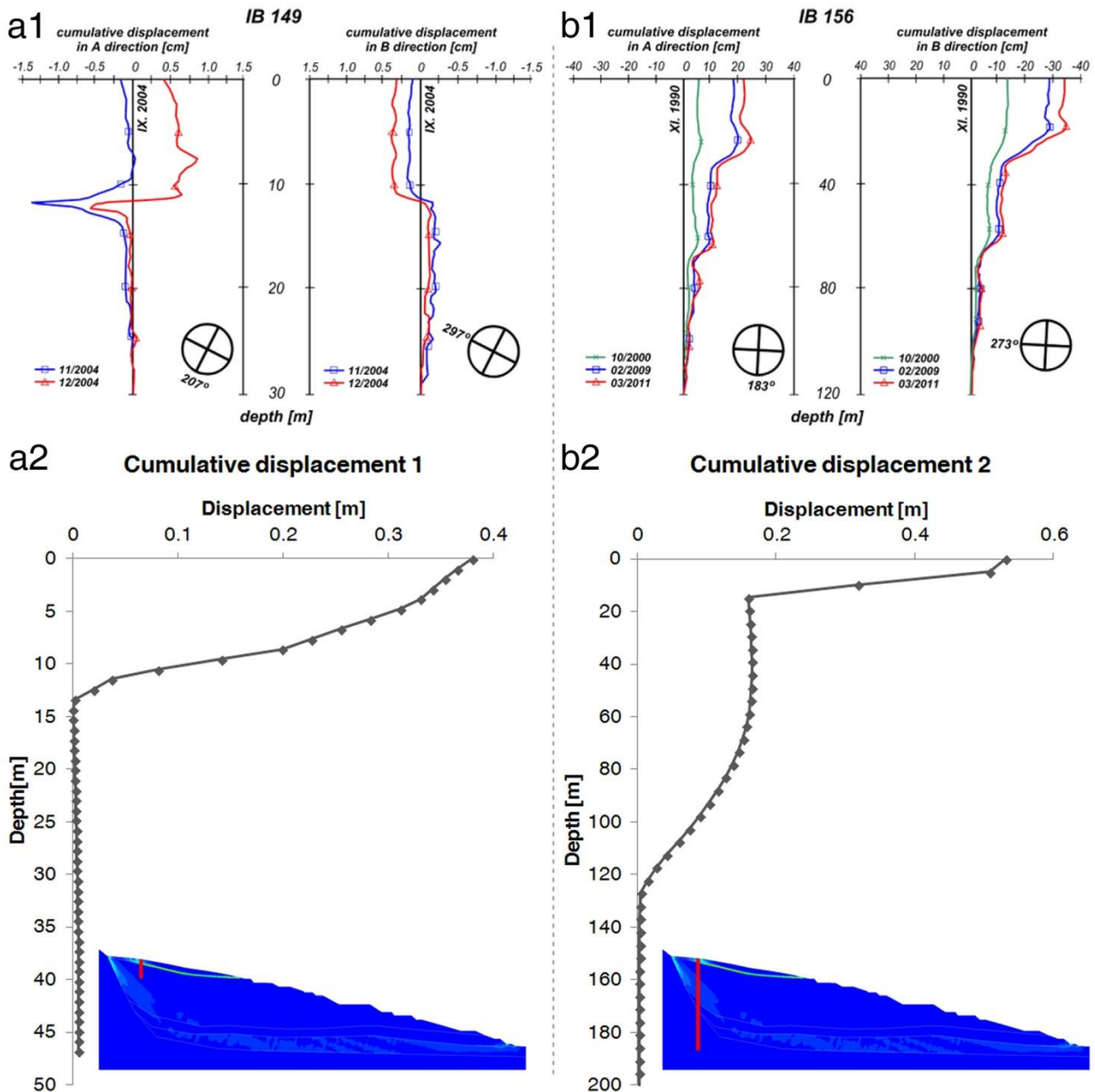


317
 318 **Fig. 9.** Shear strain development depicted in preliminary RS² numerical modelling (no vertical exaggeration is applied)
 319

320 The critical SRF value in this case is 1.09 and replicates the observed shallow landslide affecting the Quaternary
 321 sediments, indicating that the two different failure mechanisms (shallow landslide and deep-seated movements) have
 322 different FoS values of 1.35 (Fig. 8b) and 1.09 (Fig. 9), respectively.

323 To understand the reliability of these results, inclinometer data have been used for comparison. In this case, two sets of
 324 inclinometer data were selected (Fig. 10): IB149 (in the landslide area) and IB156 (near the landslide area). Locations
 325 of the two inclinometers are shown in Fig. 2. Even if the last readings date back to 2004, they still provide useful
 326 information. The IB149 inclinometer data suggest the location of a shallow landslide associated with deformation at
 327 approximately 12 m below the surface. IB156 suggests two distinct deformation horizons, one related to the shallow
 328 landslide and the other at depth that may be indicative of deep-seated instability.

329 It should be noted that the two inclinometers do not reach the same depth. IB149 (inclinometer 1), located in the
 330 landslide area, reaches a depth of only approximately 30 m whereas IB156 (inclinometer 2) reaches a depth of 120 m.
 331 The data from the two different inclinometer locations were simulated and analysed during the numerical simulation in
 332 RS². The results of the simulation are shown in Fig. 10 (data were collected in stage18, the last excavation stage). The
 333 modelled deformation reflects the shallow and deeper movements observed in the inclinometer boreholes.



334

335 **Fig. 10.** Selected inclinometer boreholes – cumulative displacement (IB 149, a1, was placed within the landslide body; IB 156, b1,
 336 was placed near the January 2011 landslide) and the results of RS² inclinometer borehole analysis 1 (a2) and 2 (b2); inset profiles
 337 show approximate inclinometer locations
 338

339 **4.2 Probabilistic FEM analysis**

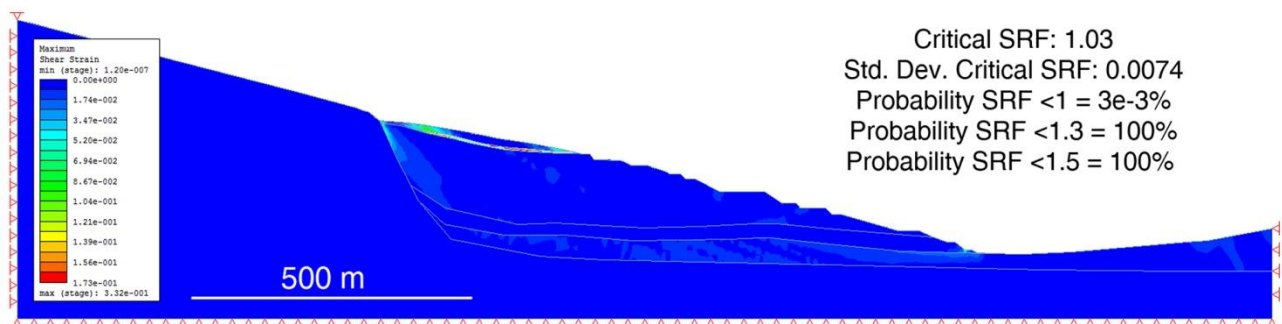
340 Given the uncertainty of the input data discussed in this report, further analyses were required. A probabilistic analysis
 341 was performed, similarly to the previous LEM sensitivity analyses, using the parameters shown in Table 4.

342 **Table 4**
 343 Statistical properties used in the probabilistic analysis for each geological formation

Material	Property	Distribution	Mean	Std. Dev.	Rel. Min.	Rel. Max.
Altered Clay	Phi (°)	Normal	9	1.33	4	4
Claystone	Phi (°)	Normal	18	1.66	5	5
Claystone	Cohesion (kPa)	Normal	100	17	50	50
Underlying complex	Phi (°)	Normal	24	1.66	5	5

344
 345 Following the same logic as the previous probabilistic analyses, the random sampling method used was the Latin
 346 Hypercube, with 1000 samples. A normal distribution was also incorporated, with SD values estimated using Equation
 347 (1).

348 The results of the probabilistic analysis are given in Fig. 11.



349
 350 **Fig. 11.** Shear strain development depicted in probabilistic RS² numerical modelling analysis (no vertical exaggeration is applied)
 351

352 Figure 11 shows a low critical SRF of 1.03 with a probability of failure of 100% considering a minimum FoS of 1.3. It
 353 should be noted that this critical SRF refers to the shallow landslide (critical area of maximum instability), but as
 354 noticed from all the simulations performed, a deeper failure surface has the potential to be activated. RS² allows
 355 consideration of a search area to define the potential location of different SRF factors, excluding the external area from
 356 the calculations. To investigate the critical SRF at an overall slope scale, a new simulation was then performed
 357 excluding the contribution of the Quaternary sediments and altered claystone layer. Utilizing this new configuration, the
 358 modelled critical SRF is 1.37, the probability of failure considering FoS < 1 is 0%, the probability of failure considering
 359 a minimum SRF of 1.3 is 0.17% and the probability of failure considering an SRF of 1.5 as a minimum acceptable
 360 value for a safe design is 100%.

361 **5 Discussion**

362 The approach adopted during the investigation utilized LEM and FEM stability analyses for the evaluation of different
363 landslide failure mechanisms affecting an open-pit lignite mine. The approach reduces uncertainty by using sensitivity
364 and probabilistic analyses to identify the critical factors that influence the results of analyses. The LEM results have
365 then been compared with the results of FEM analyses.

366 The initial sensitivity analyses based on LEM indicated that the parameters that have the greatest influence on the
367 results of the stability analyses are related to the properties of the underlying complex and claystone layers, in addition
368 to the influence of water levels on the claystone layer (Fig. 5). LEM probabilistic analysis, considering the influence of
369 water at depth, provided a minimum FoS of 1 with a probability of FoS < 1.3 of 99.2%, whereas the same analysis
370 performed excluding the effect of the presence of water at deeper levels showed a minimum FoS of 1.64 with a
371 probability of FoS < 1.3 of 0%. This latter result agrees with field observations, where no indication of a recent deep
372 failure surface is evident. In addition, the initial analyses did not replicate the presence of the shallow landslide that is
373 affecting the upper part of the slope of the ČSA mine. Analysis focused on the response of the Quaternary sediments
374 indicates an FoS of 2.1 for a possible failure surface to develop at the interface between the Quaternary and claystone
375 layers. Therefore, taking into account 2D ERT evidence and previous studies, it has been hypothesized that a weathered
376 claystone level may occur between the Quaternary sediments and the claystone layers. In the case of abundant rainfall
377 and snow melting during spring time, this altered claystone level may become saturated and water flow parallel to the
378 slope may occur at the interface with the underlying impermeable claystone. This may drastically reduce the friction
379 angle of the material, triggering potential instability (because of a *saturated infinite slope* condition). The analysis
380 shown in Fig. 7 indicates that in such a situation the FoS for the shallow Quaternary instability agrees with field
381 observations, with a minimum FoS of 0.65, a probability of FoS < 1.3 of 90.4%, and a probability of FoS < 1.5 of
382 99.6%. The results suggest that in the case of abundant precipitation, if a water flow parallel to the slope occurs because
383 of the impermeable barrier caused by the claystone, a condition of instability could be induced in the superficial strata
384 of the slope.

385 The results of FEM analyses, shown in Fig. 8, indicated that the presence of high levels of the water tables leads to a
386 low FoS value, which does not match field observations and confirms that deep water infiltration may be precluded or
387 limited by impermeable barriers in the claystone layer. In addition, the FEM analysis did not replicate the shallow
388 landslide involving the Quaternary sediments. Therefore, the analyses shown in Figs. 9, 10, and 11 were performed,
389 excluding the influence of water at depth and including the altered claystone level with low friction angle to simulate
390 the effect of water flow parallel to the slope caused by the underlying impermeable claystones. Using this configuration,
391 the presence of two possible instability mechanisms was highlighted: the development of high values of shear strain at

392 the base of the Quaternary sediments, with the possible formation of tension cracks in the upper part of the slope (lower
 393 inset map of Fig. 9) and potential development of deep-seated failure in shear within the claystones (upper inset map in
 394 Fig. 9). The critical SRF, calculated with a probabilistic approach, is 1 (Fig. 11) with a probability of failure close to 0
 395 for $SRF < 1$ and a probability of failure of 100% for $SRF = 1.3$. This refers to the critical condition of the shallow
 396 landslide, whereas the critical SRF of the deep failure surface is equal to 1.37, with a probability of $SRF < 1.3$ of 0.17%
 397 and a probability of $SRF < 1.5$ of 100%. In this case, the two failure mechanisms found in the case study area were
 398 correctly identified by FEM analysis, but different simulations had to be performed to discern the critical SRF of the
 399 two phenomena. To summarize the results obtained, and for the purpose of comparison, Table 5 shows the probability
 400 of failure using the final configuration of the model (including the altered claystone level and excluding water
 401 infiltration at depth), mean and minimum FoS values, and standard deviation of FoS (only possible with RS² software)
 402 obtained with Slide7.0 and RS². A distinction is made in Table 5, separating FoS values for the shallow and deep-seated
 403 landslides.

404 **Table 5**
 405 Comparison of Slide7.0 and RS² results in terms of FoS

Landslide	Software	Probability of failure < 1.3	Probability of failure < 1.5	Mean FoS	Minimum FoS	Std. Dev. FoS
Shallow	Slide7.0	90.4%	99.6%	1.08	0.65	–
Shallow	RS ²	100%	100%	–	1.03	0.007
Deep	Slide7.0	0%	0%	1.95	1.64	–
Deep	RS ²	0.17%	100%	–	1.37	0.02

406
 407 The results show good agreement between the different stability analyses, LEM and FEM. In detail, the FEM stability
 408 analysis appears to be more conservative for the possible deep landslide. Such results, when considering the advantages
 409 and limitations of both approaches, confirm the importance of using different methods for the interpretation of modelled
 410 results. In this case, modelled plastic deformations of the different materials appear to play an important role in
 411 simulation of the landslide, and therefore FEM analyses are particularly useful for obtaining an improved understanding
 412 of the instability mechanism.

413 The modelled results show good agreement with field observations, inclinometer data, and previous studies at the mine
 414 (Burda et al., 2011; Burda et al., 2013), confirming the reliability of the analyses performed and indicating the
 415 capability of the FEM approach to recognize different failure mechanisms in a single model. The inclinometer data
 416 were particularly useful for validation of the modelled results. From Fig. 10 it is clear how the results from modelled
 417 inclinometer 1 match what was observed in IB149, with displacements occurring at the interface between Quaternary
 418 sediments and claystones. This movement could affect the altered clay level indicated previously. In this context, it is
 419 interesting to note that a limited deeper movement (1–2 cm) is observable at depth and also illustrated in the modelled
 420 inclinometer 2. This result is similar to that of IB156, located in the vicinity of the landslide under study, in an area that

421 experienced instability problems because of deep claystone deformation in the past. Both IB156 and inclinometer 2
422 show deformation in both the deep strata and at the interface of the Quaternary sediments/claystone. Interaction
423 between the shallow and more deep-seated instability cannot be ruled out.

424 The hypothesis matches previous observations by Burda et al. (2011, 2013), which can be summarized as follows:

425 – "Immediate triggering factor for the landslide activity in the study area is the water saturation of landslide material,
426 due to a combination of high cumulative rainfall and snow melt water that results in water table increase."¹

427 – "Movement accelerations always occurred when the water table rose above -10.25m, which corresponds to a
428 theoretical pore pressure of 68 kPa at the depth of the shear plane."²

429 – "The transported and accumulated material consists primarily of Quaternary debris but also includes weathered
430 Tertiary clays (i.e., altered claystone level). This fact, along with profiles over the headscarps, indicates that the slip
431 surface passes through Tertiary claystones and that this occurs not only at the interference of Quaternary and Tertiary
432 sediments."³

433 – "Investigation revealed markedly conductive part of the claystone in the Tertiary complex. It is probable that the
434 extremely conductive part of these clays, situated at an average depth of 14 to 15 m, is conditioned by weathered and
435 water-saturated clays and represents an assumed water-bearing shear plane"⁴ whose base "is associated with high
436 resistivity zones that most likely reflect impermeable ($<10^{-8} \text{ m s}^{-1}$) dry compact claystones. This creates an ideal sliding
437 plane for the landslide (also confirmed by inclinometric boreholes)".⁵

438 In summary, the most critical condition of the slope is related to the shallow landslide activated by intense rain
439 precipitation and snow melting. According to the results of the stability analysis, it is unlikely that the effect of pore
440 pressure could trigger a superficial movement of the landslide in the Quaternary sediments. Instead, the presence of an
441 altered claystone level, immediately above the impermeable claystone layer, could provide water flow parallel to the
442 slope, decreasing the strength properties of the altered layer, leading to a condition of instability on the superficial strata
443 of the slope. Moreover, the presence of weathered Tertiary clays in the landslide accumulated debris material supports
444 this hypothesis.

445 The results of the back analysis, however, also show the possible presence of a deeper instability, which has already
446 been noted in the past in the vicinity of the area under study but could not be detected by inclinometers on the
447 reactivated landslide area because of the low depth. Because the modelled FoS of the possible deep movement is
448 between 1.3 and 1.5, further investigation is recommended to assess the likelihood and consequences of any likely

¹ Burda et al., 2011, page 1468

² Burda et al., 2013, page 372

³ Burda et al., 2011, page 1467

⁴ Burda et al., 2011, page 1471

⁵ Burda et al., 2013, page 371

449 instability. Further site investigation is also required to fully understand the water levels within the slope. In addition,
450 the application of remote sensing techniques, such as interferometry or LiDAR, would also be beneficial for monitoring
451 possible future slope displacements and validation of numerical modelling results.

452 **6 Conclusion**

453 Limit Equilibrium and Finite Element analyses have been used to assess the effects of data uncertainty for back analysis
454 of previous slope instability at a lignite operation in the Czech Republic. The case study provides valuable insight into
455 the effects of the geological parameters and model uncertainty. A sensitivity analysis was undertaken to understand the
456 controlling influences of input parameters on the model response. The results highlight that water table level and
457 material input parameters have the greatest influence on the stability of the slope. The potential for deep-seated
458 instability and shallow Quaternary sediment landsliding has been investigated. More detailed probabilistic analysis
459 suggests that a minor possibility of deep-seated instability exists.

460 The observed shallow landslide within Quaternary sediments was not initially well replicated with either Limit
461 Equilibrium or Finite Element analyses. The results of further analyses suggest that the claystone at the base of an
462 altered clay level could act as an impermeable barrier, establishing water flow parallel to the slope that decreases the
463 strength properties of the altered layer (similar to a saturated "infinite slope" condition). In this situation, the critical
464 slope angle could be approximately half that of the same dry soil, a condition sufficient to create instability. The
465 presence of weathered Tertiary clays in the landslide accumulated debris suggests that the possible shear plane involved
466 the altered claystone level. A minor possibility of deeper instability was also detected, and therefore two different
467 failure mechanisms were identified. The modelled results were shown to be in good agreement with observed
468 inclinometer data.

469 The investigation allowed an improved understanding of the landslide activity at the ČSA open-pit mine site, and the
470 increased level of knowledge provides improved hazard assessment and data for mine-planning purposes. To conclude,
471 the importance of performing sensitivity and probabilistic analyses through the approaches of Limit Equilibrium and
472 Finite Element analyses is highlighted within the analyses undertaken. Complementary use of both approaches is
473 recommended for routine checks on model response and associated results.

474 **Acknowledgements**

475 This work was supported by the Research Fund for Coal and Steel of the European Union [grant number 752504].

476 **References**

- 477 Agam, M.W., Hashim, M.H.M., Murad, M.I., Zabidi, H., 2016. Slope sensitivity analysis using Spencer's method in
478 comparison with general limit equilibrium method. *Procedia Chem.* 19, 651–658.
- 479 Alejano, L.R., Ferrero, A.M., Ramírez-Oyanguren, P., Álvarez Fernández, M.I., 2011. Comparison of limit-equilibrium,
480 numerical and physical models of wall slope stability. *Int. J. Rock Mech. Min. Sci.* 48, 16–26.
- 481 Burda, J., Žižka, L., Donhal, J., 2011. Monitoring of recent mass movement activity in anthropogenic slopes of the
482 Krušné Hory Mountains (Czech Republic). *Nat. Hazards Earth Syst. Sci.* 11, 1463–1473.
- 483 Burda, J., Hartvich F., Valenta, J., Smítka, V., Rybár, J., 2013. Climate-induced landslide reactivation at the edge of the
484 Most Basin (Czech Republic) – progress towards better landslide prediction. *Nat. Hazards Earth Syst. Sci.* 13,
485 361–374.
- 486 Cheng, Y.M., Lansivaara, T., Wei, W.B., 2007. Two-dimensional slope stability analysis by limit equilibrium and
487 strength reduction methods. *Comput. Geotech.* 34, 137–150.
- 488 Deng, D., Li, L., Wang, J., Zhao, L.H., 2016. Limit equilibrium method for rock slope stability analysis by using the
489 Generalized Hoek-Brown criterion. *Int. J. Rock Mech. Min. Sci.* 89, 176–184.
- 490 Duncan, J.M., 1996. State of the art: limit equilibrium and finite-element analysis of slopes. *J. Geotech. Eng.* 122, 577–
491 596
- 492 Duncan, J.M., 2000. Factors of safety and reliability in geotechnical engineering. *J. Geotech. Geoenviron.* 126, 307–
493 316.
- 494 Fazio, N.L., Perrotti, M., Lollino, P., Parise, M., Vattano, M., Madonia, G., Di Maggio C., 2017. A three-dimensional
495 back-analysis of the collapse of an underground cavity in soft rocks. *Eng. Geol.* 228, 301–311.
- 496 Francioni, M., Salvini, R., Stead, D., Litrico, S., 2014. A case study integrating remote sensing and distinct element
497 analysis to quarry slope stability assessment in the Monte Altissimo area, Italy. *Eng. Geol.* 183, 290–302.
- 498 Francioni, M., Salvini, R., Stead D., Giovannini, R., Riccucci, S., Vanneschi, C., Gullì D., 2015. An integrated remote
499 sensing-GIS approach for the analysis of an open pit in the Carrara marble district, Italy: Slope stability
500 assessment through kinematic and numerical methods. *Comput. Geotech.* 67, 46–63.
- 501 Francioni, M., Salvini, R., Stead, D., Coggan, J.S., 2017. Improvements in the integration of remote sensing and rock
502 slope modelling. *Nat. Hazards.*, 90(2), 975-1004.
- 503 Griffiths, D.V., Lane P.A., 1999. Slope stability analysis by finite elements. *Geotechnique* 49, 387–403.
- 504 Hurník, S., 1982. Endogenní geologické procesy a rozvoj velkolomů v severočeské hnědouhelné pánvi. *Geol. Průzk.* 5,
505 129–131 (in Czech).

506 Janbu, N., 1973. Slope stability computations. In: Hirschfeld, R.C., Poulos, S.J. (Eds.), Embankment-Dam Engineering:
507 Casagrande volume. John Wiley & Sons, Inc., New York, pp. 47–86.

508 Jiang, S.H., Huang, J., Yao, C., Yang J., 2017. Quantitative risk assessment of slope failure in 2-D spatially variable
509 soils by limit equilibrium method. *Appl. Math. Model.* 47, 710–725.

510 Klimeš, J., Baron, I., Pánek, T., Kosacík, T., Burda, J., Kresta, F., Hradecký J., 2009. Investigation of recent
511 catastrophic landslides in the flysch belt of Outer Western Carpathians (Czech Republic): progress towards
512 better hazard assessment. *Nat. Hazards Earth Sci.* 9, 119–128.

513 Ma, J.Z., Zhang, J., Huang, H.W., Zhang, L.L., Huang, J.S., 2017. Identification of representative slip surfaces for
514 reliability analysis of soil slopes based on shear strength reduction. *Comput. Geotech.* 85, 199–206.

515 Malkovský, M., 1985. Geologie severočeské hnědouhelné pánve a jejího okolí. Geology of the North Bohemian Brown
516 Coal Basin and its surroundings (in Czech). Academia, Ústřední ústav geologický, Praha, 424 pp.

517 Matsui, T., San K.C., 1992. Finite element slope stability analysis by shear strength reduction technique. *Soils Found.*
518 32, 59–70.

519 Morgenstern N.R., 1992. The evaluation of slope stability – a 25 year perspective. In: Seed, R.B., Boulanger, W.,
520 (Eds.), *Stability and performance of slopes and embankments II*. ASCE, New York, pp. 1–26.

521 Naylor, D.J., 1981. Finite elements and slope stability. In: Martin, J.B., (Ed.), *Numerical Methods in Geomechanics*.
522 Springer, Dordrecht, pp. 229–244.

523 Pánek, T., Šilhán, K., Tábořík, P., Hradecký, J., Smolková, V., Lenart, J., Brázdil, R., Kašíčková, L., Pazdur A., 2011.
524 Catastrophic slope failure and its origins: case of the May 2010 Girová Mountain long-runout rockslide (Czech
525 Republic). *Geomorphology* 130, 352–364.

526 Pichler, E., 1989. Pevnostní a přetvárné charakteristiky nezpevněných a zpevněných jílovtých hornin, Stabilita svahů
527 na povrchových hnědouhelných dolech. *Brown Coal Res. Inst.* 101–123 (in Czech).

528 Pine, R.J., 1992. Risk analysis design applications in mining geomechanics. *Trans Inst. Min. Metall.* 101(A), 149–158.

529 Pletichová, M., 2006. Hydrogeologická problematika v prostoru ochranného pilíře SKPJ. *Zpravodaj Hnědé uhlí*, 3, 12–
530 16 (in Czech).

531 Priest, S.D., Brown E.T., 1983. Probabilistic stability analysis of variable rock slopes. *Trans Inst. Min. Metall.* 92(A),
532 1–12.

533 Read, J., 2009. Data uncertainty. In: Read, J., Stacey, P., (Eds.), *Guidelines for Open Pit Slope Design*. CRC Press,
534 Balkema, pp. 213–220.

535 Rocscience, 2017a. Software products – Slide7.0, RS². www.rocscience.com.

536 Rocscience, 2017b. Slide7.0, 2D Limit Equilibrium Slope Stability Analysis. Online Help. Toronto, Canada,
537 www.rocscience.com.

538 Rybář, J., 1997. Interpretation of data about technogenic activity at the toe of Krušné Hory Mts. affecting endogenous
539 and exogenous processes in the rock environment. *Acta Montana* 106, 9–24.

540 Salvini, R., Mastrorocco, G., Esposito, G., Di Bartolo S., Coggan J.S., Vanneschi C., 2017. Use of a remotely piloted
541 aircraft system for hazard assessment in a rocky mining area (Lucca, Italy). *Nat. Hazards Earth Syst. Sci.*
542 <https://doi.org/10.5194/nhess-18-287-2018>.

543 Spreafico, M.C., Cervi, F., Francioni, M., Stead, D., Borgatti L., 2016. An investigation into the development of
544 toppling at the edge of fractured rock plateaux using a numerical modelling approach. *Geomorphology* 288,
545 83–98.

546 Stead, D., Eberhardt, E., Coggan, J.S., 2006. Developments in the characterization of complex rock slope deformation
547 and failure using numerical modelling techniques. *Eng. Geol.* 83, 217–235.

548 Tschuchnigg, F., Schweiger, H.F., Sloan, S.W., 2015. Slope stability analysis by means of finite element limit analysis
549 and finite element strength reduction techniques. Part II: Back analyses of a case history. *Comput. Geotech.* 70,
550 178–189.

551 Ugai, K., Leshchinsky D., 1995. Three-dimensional limit equilibrium and finite element analysis: a comparison of
552 results. *Soils Found.* 35, 1–7.

553 van den Ham G, Rohn J, Meier T, Czurda K (2009) Finite Element simulation of a slow moving natural slope in the
554 Upper-Austrian Alps using a visco-hypoplastic constitutive model. *Geomorphology* 103, 136–142.

555 Xie, Y., Cao, P., Liu, J., Dong L., 2016. Influence of crack surface friction on crack initiation and propagation: A
556 numerical investigation based on extended finite element method. *Comput. Geotech.* 74, 1–14.

557 Yang, X.S., Deb, S., 2009. Cuckoo search via Lévy flights. In: Abraham, A., Carvalho, A., Herrera, F., Pai, V., (Eds.),
558 *World Congress on Nature & Biologically Inspired Computing*. IEEE Publications.
559 <https://doi.org/10.1109/NABIC.2009.5393690>.

560 Zheng, Y.R., Zhao, S.Y., Kong, W.X., Deng, C.J., 2005. Geotechnical engineering limit analysis using finite element
561 method. *Rock Soil Mech.* 26,163–168.

562 Zhou, X.P. Cheng, H., 2015. The long-term stability analysis of 3D creeping slopes using the displacement-based
563 rigorous limit equilibrium method. *Eng. Geol.* 195, 292–300.

564 Zienkiewicz, O.C., Humpheson, C., Lewis R.W., 1975. Associated and non-associated visco-plasticity and plasticity in
565 soil mechanics. *Geotechnique* 25, 671–689.

566